# Magnetic structures and spin-glass-like behavior in ordered and disordered Pt-rich Pt-Mn alloys

Miwako Takahashi,[1] Timbangen Sembiring,[1,*] Yukio Noda,[2] Toetsu Shishido,[3] and Ken-ichi Ohshima[1]
[1]*Institute of Materials Science, University of Tsukuba, Tsukuba 305-8573, Japan*
[2]*Institute of Multidisciplinary Research for Advanced Materials, Tohoku University, Sendai 980-8577, Japan*
[3]*Institute for Materials Research, Tohoku University, Sendai 980-8577, Japan*
(Received 16 June 2003; revised manuscript received 3 May 2004; published 29 July 2004)

The magnetism of Pt-rich Pt-Mn alloys was studied in single crystals with different Mn concentrations (12.5, 14.4, and 15.9 at.%) and different atomic arrangements of disordered, $ABC_6$ type and $Cu_3Au$ type structures by using neutron scattering and susceptibility measurements. The neutron scattering measurements showed drastic changes in the magnetic diffraction pattern with a slight difference in the atomic arrangement and Mn concentration. In disordered alloys, magnetic diffuse peaks were observed at 1/2, 0, 0 and equivalent symmetry positions of the fcc fundamental structure. In ordered alloys with the $ABC_6$ type structure, fourfold splitting along [011] and $[0\bar{1}1]$ with incommensurate maxima appeared in the 1/2, 0, 0 diffuse scattering in Pt-12.5 at.%Mn, while the 1/2, 0, 0 diffuse scattering completely disappeared, instead, commensurate superlattice peaks were newly observed at $1/2, \pm 1/4, 0$ and $1/2, 0, \pm 1/4$ in Pt-14.4 at.%Mn. Fourfold splitting and superlattice peaks were observed with the $ABC_6$ type symmetry. In ordered alloys with the $Cu_3Au$ type structure, ferromagnetic diffuse scattering was mainly observed at the zone center of the $Cu_3Au$ type structure. The origin of these magnetic scatterings is discussed in terms of three different magnetic interactions: a spin-density wave (SDW) originated by a nesting Fermi surface, an antiferromagnetic interaction on the $ABC_6$ type structure and a ferromagnetic interaction on the $Cu_3Au$ type structure. The dominant interaction largely depends on the atomic arrangement, indicating a strong coupling between the magnetic and atomic structures in the alloys. Susceptibility measurements showed a spin-glass-like behavior in all of the samples, which is attributed to the dynamics of the fluctuating SDW clusters, as observed in other Pd-M and Pt-M (M; 3*d* element) spin-glass alloys. The persistence of the SDW fluctuations indicates the instability of these magnetic structures.

DOI: 10.1103/PhysRevB.70.014431 PACS number(s): 75.25.+z, 75.30.Fv, 75.50.Lk, 75.47.Np

## I. INTRODUCTION

The atomic phase diagram of Pt-rich Pt-Mn alloys shows quite unique ordered phases at around 12–15 at.%Mn. Our recent neutron, x-ray and electron-diffraction have revealed two ordered phases in this concentration region: a $Cu_3Au$ type ordered phase below the order–disorder transition temperature and an $ABC_6$ type ordered phase below the lower transition temperature, as described by the partial phase diagram in Fig. 1(a).[1–3] In the former structure, the corner and face-centered positions of the fcc lattice are occupied by different atoms, whereas in the latter structure, the corner positions (A and B sublattice) are occupied alternately by A and B atoms, while the face-centered positions (C sublattice) are all occupied by C atoms, as depicted in Fig. 1(b). In the ordered structure of 12.5 at.%Mn ($Pt_7Mn$) for example, A (B) is assigned as the Mn atom with B (A) and C as Pt atoms. The $ABC_6$ type structure has the unit cell $2\times2\times2$ as large as that of the fundamental fcc cell. The structure was first proposed by Tang to explain the ordered structure in Pt-Cu alloys.[4] Khachaturyan predicted that the structure can be formed from a high-temperature $Cu_3Au$ type structure as secondary ordering,[5] but until now only Pt-Mn alloys with around 12–15 at.%Mn show this double-step phase transition of the disordered state $\rightarrow Cu_3Au$ type $\rightarrow ABC_6$ type.

The magnetism in Pt-rich Pt-Mn alloys shows a spin-glass-like behavior: a cusp anomaly at the freezing temperature ($T_g$) in the magnetic susceptibility and a remanent magnetization below $T_g$, up to a Mn concentration of 16 at.%.[6] From neutron-scattering measurements on metallic spin-glass alloys of Cu-Mn, Pd-M, and Pt-M (M; 3*d* element), it is now commonly interpreted that the spin-glass-like behavior in these alloys arises from dynamical fluctuations of short-ranged spin correlations originating by a spin-density wave (SDW). In Cu-Mn alloys, the origin of the SDW is considered to be an influence of the flat Fermi surfaces normal to the [110] direction. The folding of the fcc reciprocal lattice with the flat Fermi surface brings out the SDW peaks at $1, 1/2 \pm \delta, 0$ and at symmetry-related positions. In neutron-scattering experiments, the satellite peaks are observed with a rather wide linewidth together with the atomic short-range order (ASRO) peak at 1, 1/2, 0.[7] Werner pointed out that there are 12 equivalent directions for the SDW wave vector **Q**, and complex domain configurations of the SDW with 12 choices of **Q** together with ferromagnetic clusters on the ASRO would prevent the SDW from extending across the entire crystal.[8] In Cu-Mn alloys, the atomic order can never develop to be long ranged, even by long annealing. Tsunoda *et al.* studied SDW in a Cu-Mn alloy with a well-developed ASRO, and found that a large SDW cluster grows and is stabilized through a well-defined Fermi surface in a long-period superstructure, resulting in a higher $T_g$ in the alloy.[9] In inelastic neutron scattering studies, it has been revealed that the SDW diffuse scattering consists of elastic and inelastic components.[10–13] The elastic component tends to be zero near $T_g$, whereas a strong inelastic component persists far

 

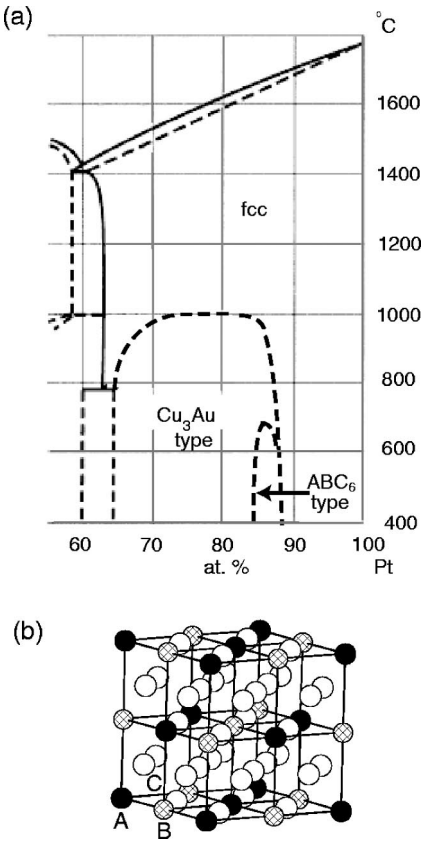


FIG. 1. (a) Partial phase diagram of the Pt-rich Pt-Mn alloy. (b) Structure of the $ABC_6$ type order.

above $T_g$. The inelastic component is ascribed to dynamical fluctuations of the SDW cluster, which persist above $T_g$ with their time-averaged amplitudes being zero. These results point out that the fluctuating SDW clusters play an essential role in the spin-glass-like behavior.

In Pd-M and Pt-M alloys, SDW peaks appear at $1\pm\delta$, 0, 0 and its equivalent positions, where $\delta$ varies continuously with changing the concentration of the 3*d* element.[14–19] The shift of SDW peaks is explained as being the result of an expansion of the hole Fermi surface due to an increase of the M concentration. However, the Pt-Mn alloy system is an exception. In the alloys, peaks are always observed at $1\pm\delta,0,0$ with $\delta=1/2$ throughout the Mn concentration from 3 to 13 at. %.[19–21] The peak position in the Pd-M and Pt-M alloys reflects the shape of the Fermi surface of Pd or Pt host metal, both of which are similar to each other with nearly parallel planes normal to the cubic axis.[22] Since the formation of the SDW is due to the characteristic shape of the Fermi surface of the host Pt or Pd metal, studies on Pt-M and Pd-M alloys have been concentrated on disordered alloys with a low M concentration. For alloys with a higher M concentration, most of them form a $Cu_3Au$ type atomic order around 25 at. %, and the SDW cluster is taken over by the magnetic structure on the atomic order. However, considering that the Pt-Mn alloys have very unusual phase diagram in a region of rather low Mn concentration, magnetism in the alloys is expected to be different from that of other Pt-M and Pd-M alloys. The persistence of the SDW peak positions at $1\pm1/2$, 0, 0 would be related to the atomic orders in the alloys. Based on the idea, we have performed magnetic susceptibility and neutron-diffraction measurements on Pt-rich Pt-Mn alloys. The aim of the studies has been to elucidate the relation between the atomic order and magnetism in Pt-Mn alloys, especially between the $ABC_6$ type order and SDW.

In this paper, we present experimental results on Pt-Mn alloys with different Mn concentrations of 12.5, 14.4, and 15.9 at. %, which have atomic-ordered phases of both $Cu_3Au$ and $ABC_6$ type structures. By changing the heat treatments of the samples, we studied the magnetism in samples with eight different atomic arrangements: an atomic long-range order (ALRO) of either the $Cu_3Au$ or $ABC_6$ type structure, or ASRO of these structures with different correlation lengths. The detailed atomic arrangements are described in Sec. II. In Sec. III, we show the results that the magnetic structure changes largely with a slight difference in the atomic arrangement, and that the spin-glass-like behavior survives throughout all of the samples. The interactions of the magnetic structures and effects of the atomic order on the magnetism are discussed in Sec. IV. Conclusion is given in Sec. V.

## II. EXPERIMENTAL PROCEDURES

Three single crystals of 12.5, 14.4, and 15.9 at.%Mn were grown using the Bridgman technique at the Institute for Materials Research, Tohoku University. Cylindrical samples of about 10 mm height and diameter were used for neutron-scattering measurements. Small rectangular samples were also cut from the same ingots for magnetic-susceptibility measurements. The compositions of the samples were determined by an electron probe microanalysis (EPMA) technique at the Chemical Analysis Center, University of Tsukuba. In order to achieve different atomic arrangements for each sample, they were quenched, or annealed, with different annealing processes, as summarized in Table I.

The atomic arrangements of the samples were characterized by the intensities and peak profiles of reflections at the superlattice points in the neutron-diffraction data. In this paper, although the unit cell of the $ABC_6$ type structure is $2\times2\times2$ as large as that of the fundamental and $Cu_3Au$ type structures, the latter lattice is used for convenience. In the ordered structure, superlattice reflections appear at the X points of an fcc lattice, such as 100 and 110 for the $Cu_3Au$ type order, and at the L points of the fcc lattice, such as $1/2$, $1/2$, $1/2$, together with the X-point reflections for the $ABC_6$ type order. While the former structure is described with one order parameter ($S$), the latter one needs two independent order parameters ($S_1$ and $S_2$). $S_1$ is related to the degree of the $Cu_3Au$ type order, while $S_2$ is related to that of a NaCl type order formed by alternate occupation of the A and B atoms at the corner sites in the fcc lattice. The magnitudes of the order parameters ($S_1$, $S_2$, and $S$) were obtained from the intensity ratio of the X- and L-points superlattice reflections to the fundamental reflection.

The correlation lengths of the ASRO were estimated by fitting the profiles of diffuse peaks at the superlattice points

TABLE I. Process of heat treatments for the samples.

| | | | |
|---|---|---|---|
| 12.5 at.%Mn | Quenched | | 850°C→RT |
| | Annealed | #1 | 1000°C→400°C for 4 days→RT |
| | Annealed | #2 | 1000°C→slowly cooled down to 400°C for 1 month→RT |
| 14.4 at.%Mn | Quenched | | 1000°C→RT |
| | Annealed | #1 | 1000°C→650°C for 4 days→RT |
| | Annealed | #2 | 1000°C→slowly cooled down to 400°C for 1 month→RT |
| 15.9 at.%Mn | Quenched | | 1000°C→RT |
| | Annealed | | 1000°C→slowly cooled down to 400°C for 1 month→RT |

with a resolution-convoluted Lorentz function. In the present alloys, ASRO is complicated because the profiles at the X and L points appear differently. Therefore, two correlation lengths, $\xi_X$ and $\xi_L$, were estimated for the X- and L-point diffuse peaks, respectively. In some samples, a sharp peak and weak broad diffuse scattering were observed simultaneously at the same superlattice point. We regard such reflections as indicating that there is a well-developed ASRO related to the points. The correlation length for the well-developed ASRO is larger than the scale that we can detect by the present measurements, which is about $70a_0$ ($a_0$ is a lattice parameter of the fcc fundamental unit cell and $\sim$3.9 Å). The X-point reflections in the quenched samples of 14.4 and 15.9 at.%Mn and the L-point reflections in the annealed 15.9 at.%Mn show such peak profiles of well-developed ASRO. When the sample is annealed at the temperature of the $Cu_3Au$ ordered phase, resolution-limited peaks are observed at the X point, while L-point reflections are still broad diffuse peaks. We take these sample as being the $Cu_3Au$ type ordered state with the $ABC_6$ type ASRO, and estimate $S$ for the ordered structure and $\xi_L$ for the ASRO. This is the case for the annealed #1 sample of 14.4 at.%Mn and the annealed 15.9 at.%Mn sample. We summarize the atomic arrangement for the measured samples with the order parameter $S_1$, $S_2$ or $S$ for the ALRO and the correlation length $\xi_X$, $\xi_L$ for the ASRO in Table II. The resultant atomic arrangements are almost consistent with those expected from the heat treatments.

Neutron-scattering measurements were carried out using two diffractometers: FOX installed at the pulsed spallation-neutron source, KENS, at the High Energy Accelerator Research Organization (KEK) and FONDER, recently installed at the T2-2 beam port of the thermal guide at the JRR-3M research reactor at the Japan Atomic Energy Research Institute (JAERI). FOX uses a time-of-flight (TOF) Laue technique by combining the TOF method with white neutrons and a multidetector system of 36 linearly placed $^3$He detectors.[23] The spectrometer enables us to observe a large area of two-dimensional reciprocal space with a single measurement. For the TOF spectra obtained at FOX, the wavelength dependence of the incident neutron flux is corrected by incoherent scattering from a vanadium specimen. The

TABLE II. Atomic arrangement for the samples. $S_1$ and $S_2$ are order parameters for the $ABC_6$ type order, $S$ is that of the $Cu_3Au$ order and $\xi_X$, $\xi_L$ are the correlation lengths of ASRO related to the X- and L-point diffuse scattering, respectively. $a_0$ is the lattice parameter of the fundamental fcc unit cell.

| | | | |
|---|---|---|---|
| 12.5 at.%Mn | Quenched | | ASRO with $\xi_X=10a_0$, $\xi_L=6a_0$ |
| | Annealed | #1 | $ABC_6$ type order with $S_1=0.8$, $S_2=0.5$ |
| | Annealed | #2 | $ABC_6$ type order with $S_1=0.9$, $S_2=0.7$ |
| 14.4 at.%Mn | Quenched | | Well-developed $Cu_3Au$ type ASRO ($\xi_X>70a_0$) and $ABC_6$ type ASRO with $\xi_L=10a_0$ |
| | Annealed | #1 | $Cu_3Au$ type order with $S=0.6$ and $ABC_6$ type ASRO with $\xi_L=35a_0$ |
| | Annealed | #2 | $ABC_6$ type order with $S_1=1$, $S_2=0.7$ |
| 15.9 at.%Mn | Quenched | | Well-developed $Cu_3Au$ type ASRO ($\xi_X>70a_0$) and $ABC_6$ type ASRO with $\xi_L=5a_0$ |
| | Annealed | | $Cu_3Au$ type order with $S=0.5$ and well-developed $ABC_6$ type ASRO ($\xi_X>70a_0$) |

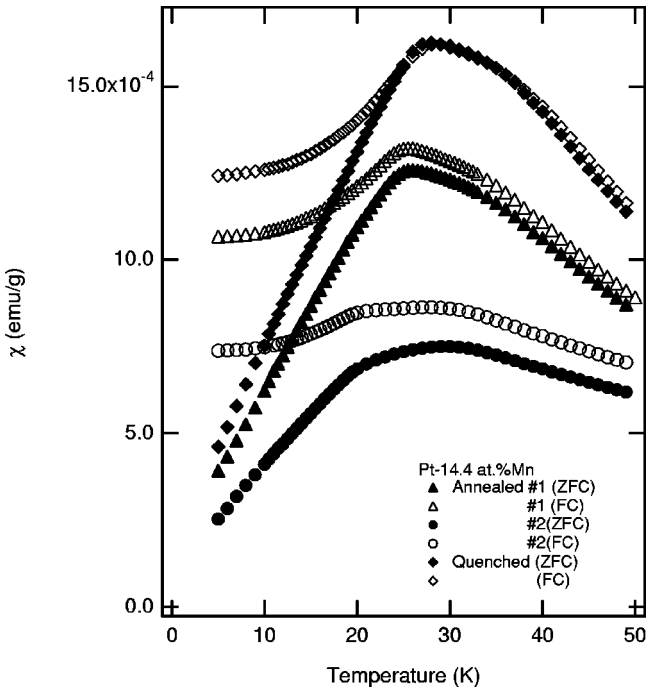


FIG. 2. Temperature dependence of the dc magnetic susceptibility for the samples of 14.4 at.%Mn. ZFC and FC indicate that the samples were cooled in a zero field and in a field of 100 Oe, respectively.

scattered intensities are also normalized by the total count of a monitor placed on the incident neutron pass. FONDER is a four-circle diffractometer with monochromatized neutrons, and it is thus possible to measure three-dimensional intensity distributions.[24] In measurements with FONDER, the data were taken with incident neutron wavelengths of 2.44 Å of PG(002), 1.57 Å of Si(422) and 1.54 Å of Ge(511).

The magnetic susceptibility was also measured using a superconducting quantum interference device (SQUID) in the temperature range between 5 to 300 K under a magnetic field of 100 Oe.

## III. EXPERIMENTAL RESULTS

### A. Magnetic susceptibility

The temperature dependence of the magnetic susceptibility, $\chi(T)$, of each sample was measured under a magnetic field of 100 Oe after being zero-field cooled (ZFC) and field cooled (FC). For all samples, $\chi(T)$ shows the spin-glass-like behavior with different features, depending on Mn concentration and atomic order. For the same Mn concentration, $T_g$ becomes lower and $\chi(T_g)$ tends to be smaller in the annealed samples than in the quenched ones. The cusp is quite sharp in 12.5 at.%Mn, but smeared in 15.9 at.%Mn. Figure 2 shows $\chi(T)$ of 14.4 at.%Mn. It is noted that for the annealed #2 sample, the cusp is not apparent and an antiferromagnetic transition-like anomaly is observed at 20 K for both the FC and ZFC process. We regard the anomaly as being due to the formation of an antiferromagnetic order in the sample at a Néel temperature of $T_N$=20 K. In the sample, the remanence was observed from room temperature (RT). The maximum susceptibility at $T_g$, $\chi(T_g)$, and the freezing temperatures estimated from the cusp position, together with the Néel temperature and $\chi(T_N)$ for the annealed #2 sample of 14.4 at.%Mn, are listed in Table III.

TABLE III. Freezing temperature, $T_g$, and $\chi(T_g)$ obtained from the magnetic susceptibility for eight samples.

| | | | $T_g$ | $\chi(T_g)$ $\times 10^{-4}$ (emu/g) |
|---|---|---|---|---|
| 12.5 at.%Mn | Quenched | | 23 K | 2.6 |
| | Annealed | #1 | 20 K | 3.7 |
| | Annealed | #2 | 16 K | 0.7 |
| 14.4 at.%Mn | Quenched | | 28 K | 16 |
| | Annealed | #1 | 26 K | 13 |
| | Annealed | #2 | $T_N$=20 K | 7.2($\chi(T_N)$, ZFC) 8.5($\chi(T_N)$, FC) |
| 15.9 at.%Mn | Quenched | | 30 K | 20 |
| | Annealed | | 27 K | 11 |

### B. Neutron diffraction

In quenched samples of 12.5 and 14.4 at.%Mn, SDW diffuse peaks were observed at 1/2,0,0 and equivalent points of the fcc fundamental structure, as previously reported for disordered Pt-Mn alloys. The correlation lengths for these diffuse peaks estimated by fitting the profile at 1/2,0,0 with a Lorentz function are $12a_0$ and $15a_0$ for 12.5 and 14.4 at.%Mn, respectively.

The diffraction pattern in the (001) scattering plane at 4 K in the annealed #1 sample of 12.5 at.%Mn is shown in Fig. 3(a). The data were collected at FOX. In this and the following imaged diffraction patterns, the logarithmic intensities are plotted to emphasize weak diffuse scattering. The intensities distributed circularly at 1.6 and 1.8 reduced lattice unit (r.l.u.) are due to powdered Bragg lines of Al(111) and Al(200), respectively, both of which come from a sample stage. As seen in the figure, the characteristic fourfold splittings of diffuse scattering appear at 1/2, 1/2, 0 and 1/2, 3/2, 0. It should be noted that the positions are equivalent to the 1/2, 0, 0 in the $ABC_6$ type structure, but not equivalent in the disordered and $Cu_3Au$ type structures, and no magnetic peaks appear at these points in the quenched samples. The four maxima of the splitting are separated along the diagonal directions of [110] and $[1\bar{1}0]$. The intensities of the split maxima in the 1/2, 1/2, 0 diffuse scattering are $\sim 10^{-3}$ of that of the 111 fundamental reflections. At 1/2,1,0, 1/2, 2, 0, and 3/2, 2, 0, twofold splittings of diffuse scattering appear along [010], and at 1, 3/2, 0 along [100]. They appear at around the points equivalent to 1/2, 0, 0 in the $ABC_6$

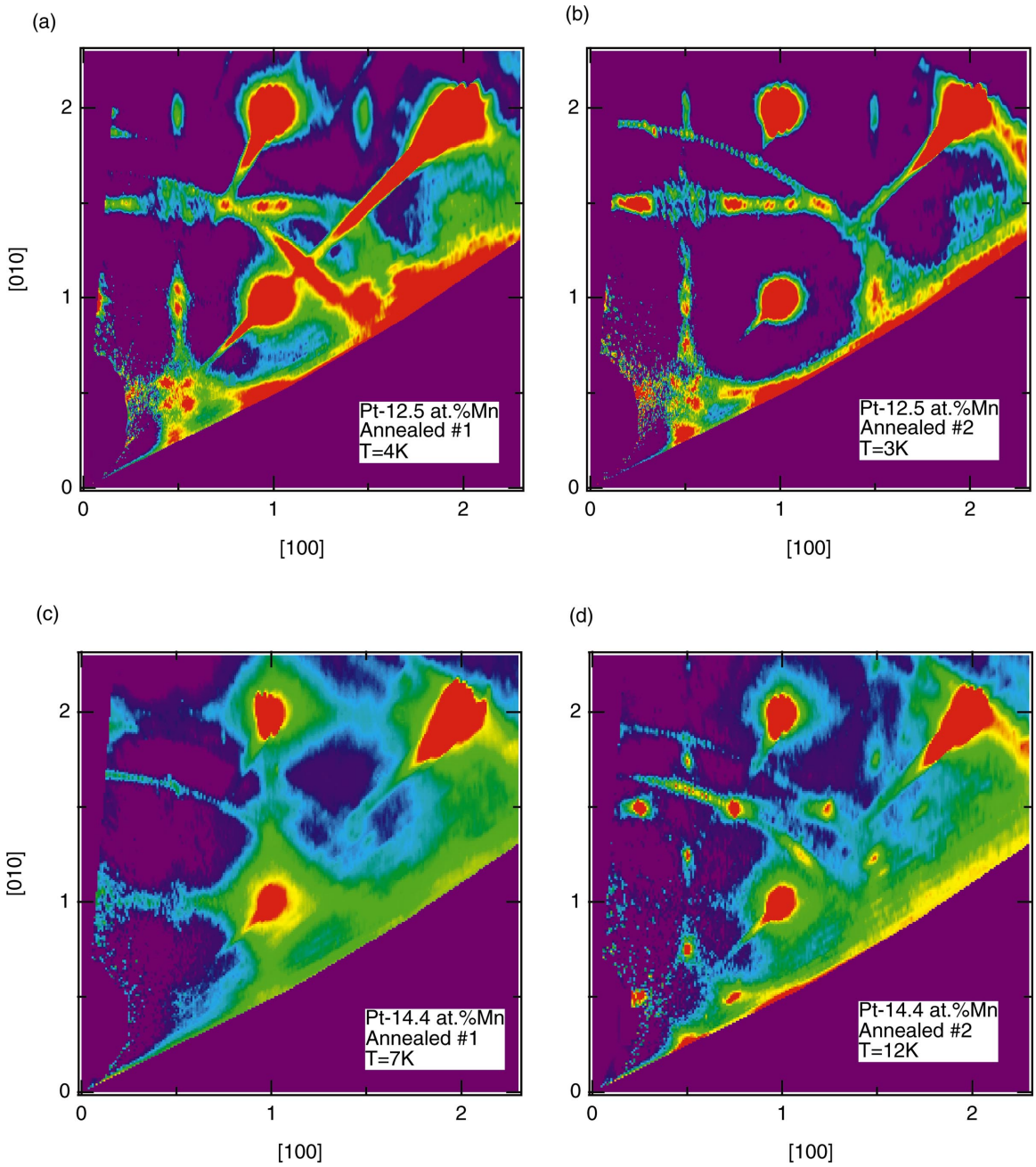


FIG. 3. (Color) Diffraction patterns on the (001) scattering plane measured at FOX; (a) for the annealed #1 sample of 12.5 at.%Mn at 4 K, (b) for the annealed #2 of 12.5 at.%Mn at 3 K, (c) for the annealed #1 sample of 14.4 at.%Mn at 7 K, and (d) for the annealed #2 sample of 14.4 at.%Mn at 12 K.

type structure, and the separation of the splitting is the same as that of the fourfold splitting at $1/2, 0, 0$ along the cubic axis. Considering that the vertical resolution of FOX is not sufficient, the twofold splittings are regarded as projections of fourfold splittings of diffuse scattering spread in the planes vertical to the (001) scattering plane. At $1/2, 0, 0$, the splitting of diffuse scattering was also observed with its intensities more than twice as strong as that of the diffuse scattering at the same point in the quenched sample of 12.5 at.%Mn. The diffuse scattering remains at 25 K, though the intensities are much lower and the splittings are smeared.

The detailed structure of the diffuse scattering was investigated in the narrowed three-dimensional reciprocal space at FONDER. The intensity distribution around $1/2, 0, 0$ shows four maxima at $1/2, \pm 0.06, \pm 0.06$ and $1/2, \pm 0.06, \mp 0.06$. The diffuse intensities spread widely on the plane vertical to [100] and narrowly along the direction with the FWHM being $\sim 0.1$ r.l.u. A fourfold splitting of diffuse scattering was also observed at around $0, 1, 1/2$ on the (001) plane in the

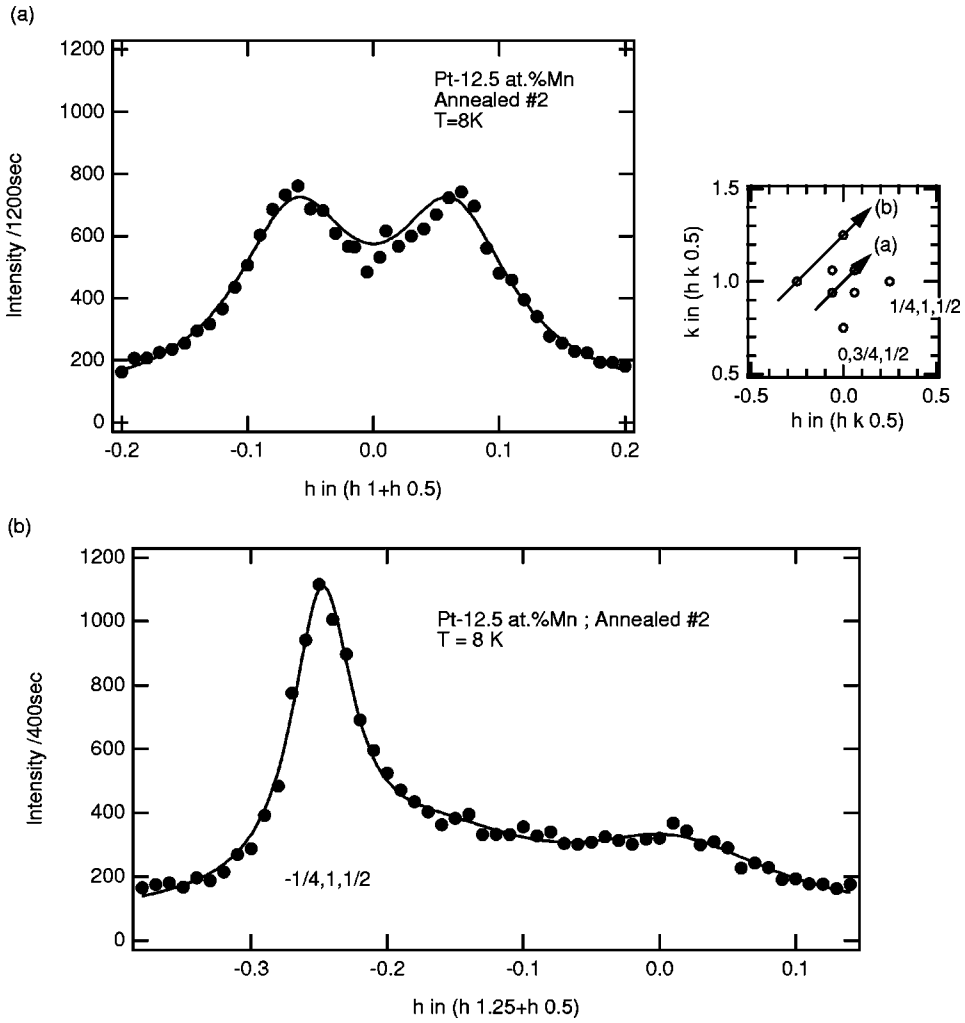


FIG. 4. Diffraction line profile parallel to [110] through (a) $0,1,1/2$ and (b) $-1/4,1,1/2$ and $0,5/4,1/2$ at 8 K measured on the annealed #2 sample of 12.5 at.%Mn at FONDER. The diagram for scans (a) and (b) is plotted together.

same way. These data indicate that the $1/2$, 0, 0 diffuse scattering spreads two dimensionally on the (100) plane with a fourfold splitting, and appears at the equivalent points of the $ABC_6$ type structure.

The diffraction pattern in the (001) scattering plane at 3 K for the annealed #2 sample of 12.5 at.%Mn is shown in Fig. 3(b). In the figure, twofold and fourfold splittings of diffuse scattering are similarly observed as in Fig. 3(a). The remarkable change is that additional diffuse peaks appear at $1/2,1/2\pm1/4,0$, $1/2\pm1/4,1/2,0$, etc. These positions are equivalent to each other in the $ABC_6$ type structure. Both the newly appearing diffuse peaks and the split diffuse scattering decrease their intensities with increasing temperature, but still remain at 25 K.

The profiles of the magnetic peaks in an annealed #2 sample of 12.5 at.%Mn were studied at FONDER. Figures 4(a) and 4(b) show line profiles of the peaks around $0,1,1/2$ at 8 K. A diagram of the scans is also shown in the figures. Figure 4(a) shows an intensity profile on the [110] line through $0,1,1/2$. Split maxima of diffuse scattering appear at $\pm0.06,1\pm0.06,1/2$. The profile was found to be quite similar to that in the annealed #1 sample of 12.5 at.%Mn. Figure 4(b) shows the profile on the line passing through $-1/4,1,1/2$ and $0,5/4,1/2$, which are the equivalent points where magnetic peaks are newly observed. The intensity distribution is quite anisotropic. It is about 10 times stronger at $-1/4,1,1/2$ than at $0,5/4,1/2$, and the width of the latter peak is much broader than that of the former. The peak intensity at $-1/4,1,1/2$ is nearly twice as strong as those at $\pm0.06,1\pm0.06,1/2$. The correlation lengths for these diffuse peaks were estimated by fitting the profiles with a resolution convoluted Lorentz function. The correlation length was also estimated for the peaks at $\pm0.06,1\pm0.06,1/2$ in the annealed #1 sample of 12.5 at.%Mn in the same way. The resultant values for the peaks at $\pm0.06,1\pm0.06,1/2$ are $\sim18a_0$ and $\sim16a_0$ for the annealed #1 and #2 samples of 12.5 at.%Mn, respectively. For the peak at $-1/4,1,1/2$, it is $\sim30a_0$, while $\sim7a_0$ for $0,5/4,1/2$.

Figure 5 shows the temperature dependences of the magnetic intensities in Pt-12.5 at.%Mn samples, normalized by their maxima at the lowest temperature. They are plotted for the diffuse scattering at $1/2,0,0$ in the quenched and annealed #1 samples, and those at $0,1,1/2$ and at $-1/4,1,1/2$ in the annealed #2 sample. They all increase at lower temperature rapidly with a tail extending to higher temperature. The tail is longest for the $1/2,0,0$ peak in the quenched sample, extending up to RT, and shortest for the $-1/4,1,1/2$ peak in the annealed #2 sample. The temperatures below which the intensities increase remarkably are $\sim100$ K and $\sim60$ K for the $1/2,0,0$ peak in the quenched and annealed #1 samples, $\sim40$ K and $\sim20$ K for the $0,1,1/2$ and

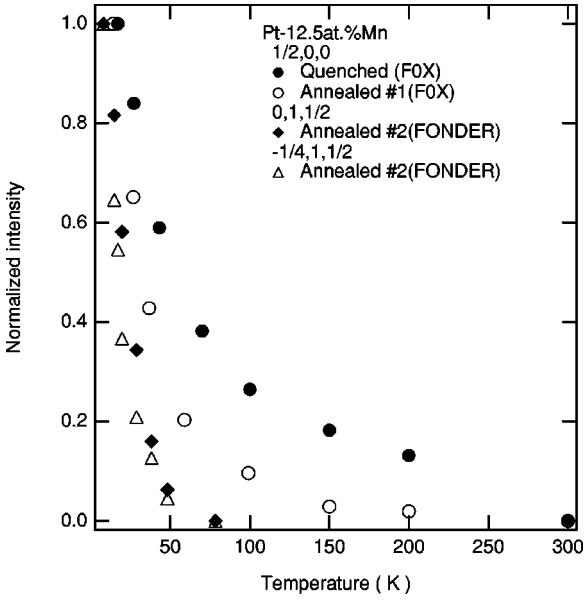


FIG. 5. Temperature dependence of the normalized magnetic intensity of the diffuse scattering in the 12.5 at.%Mn samples: at $1/2,0,0$ in the quenched sample (●) and the annealed #1 sample (○), at $0,1,1/2$ (◆) and $-1/4,1,1/2$ (△) in the annealed #2 sample.

$-1/4,1,1/2$ peak in the annealed #2 sample, respectively. No anomaly is found at $T_g$ for these temperature dependences.

The diffraction pattern in the (001) scattering plane at 7 K for the annealed #1 sample of 14.4 at.%Mn is shown in Fig. 3(c). The diffuse intensities at $1/2,1/2,0$ and at its equivalent points of the $ABC_6$ type structure are very weak, but have the same anisotropic distributions as in Figs. 3(a) and 3(b). On the other hand, no peaks are seen at $1/2,3/4,0$ and its equivalent points of the $ABC_6$ type structure. In Fig. 6(a), the temperature dependence of the normalized magnetic diffuse intensities at around $1/2,0,0$ is shown for the annealed #1 and quenched samples of 14.4 at.%Mn. The figure shows a remarkable resemblance in the temperature dependence between the two samples. The intensities increase with decreasing temperature below around 80 K with tails extending up to 300 K, and have no anomaly at $T_g$.

The diffraction pattern changes drastically in the annealed #2 sample of 14.4 at.%Mn, as shown in Fig. 3(d). Diffuse scattering at around $1/2,1/2,0$ disappears completely, and instead, superlattice reflections appear at $1/2,1/2\pm1/4,0$, $1/2\pm1/4,1/2,0$ and their equivalent points in the $ABC_6$ type structure. The peak intensity at $1/2,3/4,0$ was found to be $\sim10^{-2}$ of that of the 111 fundamental reflection, and the width corresponds to a resolution-limited value. Its temperature dependence is shown in Fig. 6(b). The intensity decreases rapidly with increasing temperature, and almost disappears at 20 K, where an antiferromagneticlike anomaly was found in a magnetic-susceptibility measurement. It is thus confirmed that a long-range order of antiferromagnetic modulation is formed below $T_N=20$ K in the annealed #2 sample of 14.4 at.%Mn.

The profile of the magnetic peaks at around $0,1,1/2$ in the annealed #2 sample of 14.4 at.%Mn was studied at

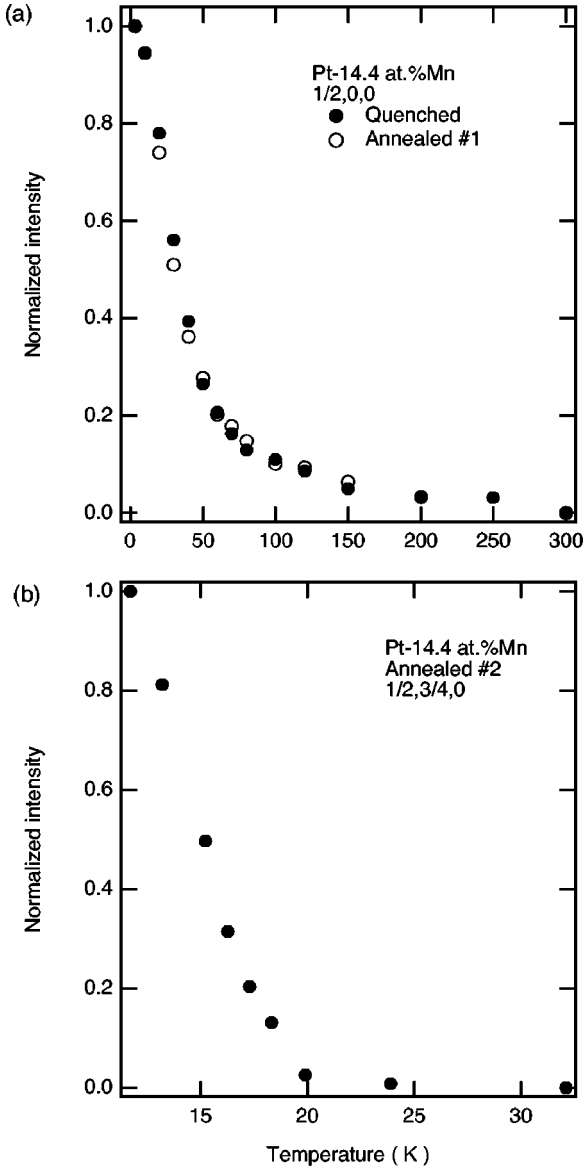


FIG. 6. Temperature dependence of the normalized magnetic intensity in the 14.4 at.%Mn samples measured at FOX: (a) for the diffuse scattering at $1/2,0,0$ in the quenched sample (●) and annealed #1 sample (○) and (b) for the superlattice reflection at $1/2,3/4,0$ in the annealed #2 sample.

FONDER. From a measurement at 8 K, we found that the intensities of the magnetic superlattice reflections at $0,1\pm1/4,1/2$ and $\pm1/4,1,1/2$ are quite different; the intensities at $\pm1/4,1,1/2$ are more than three times stronger compared with those at $0,1\pm1/4,1/2$. The result indicates that they come from different magnetic domains. Figure 7 shows a contour map on the (001) scattering plane centered at $0,1,1/2$ at 40 K. In this figure, we assumed two mirror planes along [110] and $[1\bar{1}0]$, and made a fourfolded pattern from the measured one inside the dotted lines. The figure shows that even at $2T_N$, magnetic intensities still remain at the superlattice points, though their intensities are less than $10^{-3}$ of those below $T_N$.

In samples with an ALRO or a well-developed ASRO of the $Cu_3Au$ type structure, i.e., in the quenched and annealed

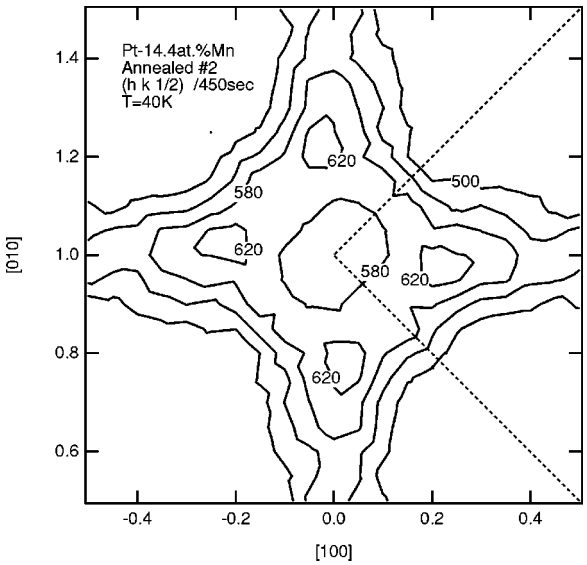


FIG. 7. Scattering intensity contour map around $0,1,1/2$ on the (001) scattering plane at 40 K measured on the annealed #2 sample of 14.4 at. % Mn at FONDER. The dotted lines show the measured area.

#1 samples of 14.4 at.%Mn and quenched and annealed samples of 15.9 at.%Mn, broad diffuse peaks due to the ferromagnetic correlation on the $Cu_3Au$ type order were observed. The observed magnetic scattering in the present samples is quite complicated. For a better understanding, it is summarized in Table IV.

## IV. DISCUSSION

### A. Magnetic structure

In samples with the $ABC_6$ type structure, there are two characteristic magnetic scatterings, i.e., the fourfold splitting of diffuse scattering in the 12.5 at.%Mn and the superlattice peaks in the 14.4 at.%Mn sample, as shown in Figs. 8(a) and 8(b), respectively.

The fourfold splitting of diffuse scattering appears at $1/2,0,0$ with maxima at $1/2,\pm 0.06,\pm 0.06$ and $1/2,\pm 0.06,\mp 0.06$, and equivalent points of the $ABC_6$ type structure. It should be noted that the splitting is centered at $1/2,0,0$, which is the zone boundary (zb) of the $ABC_6$ type structure. The magnetic structure is thus regarded to have an antiparallel alignment for successive (100) planes of the Mn atoms, with an incommensurate modulation of the period of about $17a_0$ parallel to the diagonal direction in the plane. Since its temperature dependence is similar to that observed for the SDW diffuse scattering, the origin is also attributed to SDW formation. We consider the SDW formed on the $ABC_6$ type structure to have originated through an enhanced nesting Fermi-surface effect, as follows. Figures 9(a) and 9(b) show schematic descriptions of the reciprocal lattice of the fundamental fcc and the $ABC_6$ type structures, respectively. We assume that the shape of the Fermi surface is the same as that of Pt in both structures, then it has a set of nearly parallel planes normal to the cubic axis.[25] In the figures, **Q** is a wave-vector spanning the flat Fermi surfaces, which is nearly along [100] with its magnitude $|\mathbf{Q}| \sim 1/2$ r.l.u. In Fig. 9(a), which corresponds to the disordered state, the SDW peaks appear at the terminal points of **Q** starting from the fcc reciprocal lattice points (on the dotted line in the figure), which are around $\pm 1/2,0,0$ and their equivalent points. On the other hand, in Fig. 9(b), the Brillouin zones (BZ) of the $ABC_6$ structure become smaller and $\pm\mathbf{Q}$ from the nearest reciprocal points cross each other at their terminal points. As a result, the effect of Fermi-surface nesting is approximately doubled at the crossing, giving rise to enhanced intensities in the SDW scattering. Considering that the system is three dimensional, the direction of the nesting vector **Q** is not strictly along the cubic axis and the crossing points spread on

TABLE IV. Magnetic scattering observed for eight samples. For each scattering, the dominant interaction is indicated as SDW, antiferromagnetic (AF) or ferromagnetic (F) interaction.

| | | | |
|---|---|---|---|
| 12.5 at.%Mn | Quenched | | Diffuse scattering at $1/2,0,0$ (SDW) |
| | Annealed | #1 | Diffuse scattering with fourfold splitting at $1/2,0,0$ (SDW) |
| | Annealed | #2 | Diffuse scattering with fourfold splitting at $1/2,0,0$ (SDW) |
| | | | Diffuse scattering at $1/2,\pm 1/4,0$ and $1/2,0,\pm 1/4$ (AF) |
| 14.4 at.%Mn | Quenched | | Diffuse scattering at $1/2,0,0$ (SDW) |
| | | | Weak diffuse scattering at 100 (F) |
| | Annealed | #1 | Diffuse scattering at $1/2,0,0$ on (100) plane (SDW) |
| | | | Weak diffuse scattering at 100 (F) |
| | Annealed | #2 | Superlattice refections at $1/2,\pm 1/4,0$ and $1/2,0,\pm 1/4$ (AF) |
| 15.9 at.%Mn | Quenched | | Diffuse scattering at 100 (F) |
| | Annealed | | Diffuse scattering at 100 (F) |

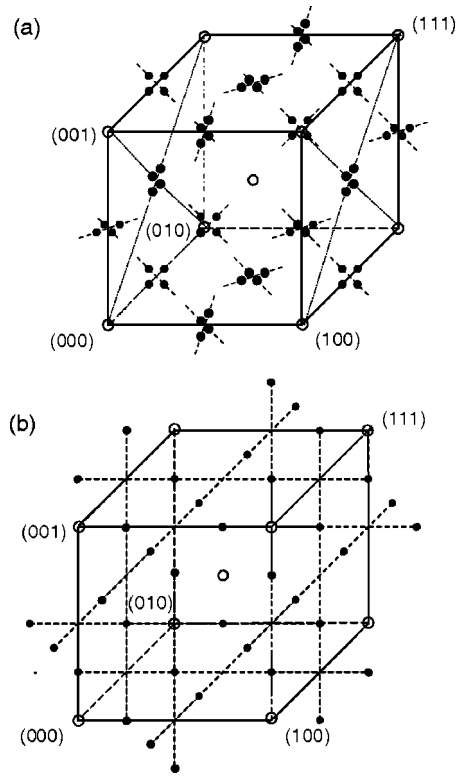


FIG. 8. (a) Fourfold splittings of the diffuse scattering at $1/2,0,0$ and its equivalent positions of $ABC_6$ type structure, observed in the annealed samples of 12.5 at.%Mn. (b) Magnetic superlattice reflections at $1/2,\pm 1/4,0$, $1/2,0,\pm 1/4$ and their equivalent positions of $ABC_6$ type structure, observed in the annealed #2 sample of 14.4 at.%Mn. Open and closed circles indicate nuclear and magnetic scattering, respectively.

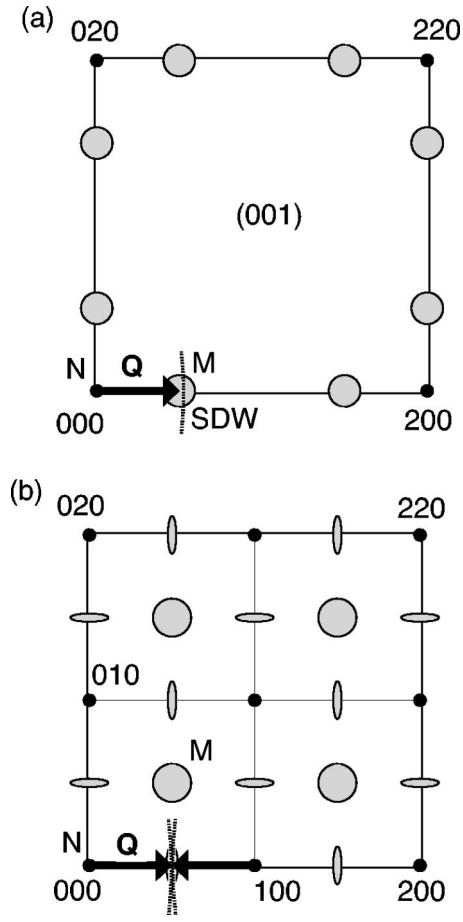


FIG. 9. Nesting Fermi-surface effects on the (001) reciprocal lattice planes of (a) the fundamental fcc structure and (b) the $ABC_6$ type structure. The closed circles indicate the fundamental and the $ABC_6$ type superlattice reflections; the dotted lines indicate sets of terminal points of the SDW wave vector, **Q**. The shaded areas indicate the magnetic diffuse scattering.

the plane normal to [100] around $\pm 1/2,0,0$. Accordingly, the SDW diffuse intensities become stronger with anisotropic distributions as in Fig. 9(b). The model well explains the observed diffraction pattern in Fig. 3(a), except for the fourfold splitting in the diffuse scattering, which indicates a quite complicated structure of the nesting Fermi surface in the actual ordered alloy.

The model of the enhancement of the Fermi-surface nesting effect is based on the Fermi-surface-imaging theory proposed by Moss to explain the fourfold splitting in the diffuse scattering observed in the electron and x-ray diffraction patterns in Cu-Au alloys.[26] In the Cu-Au alloys, the direction of the vector spanning the flat Fermi surface is nearly along [110], and four ASRO peaks appear at $1,1\pm\delta,0$ and $1\pm\delta,1,0$ due to the fourfold degeneracy in the direction of the vector. This also explains the magnetic peaks at $1,1/2\pm\delta,0$ in Cu-Mn alloys. However, it should be emphasized that in the present samples, the Fermi-surface nesting effect is not enhanced until the atomic structure forms the $ABC_6$ type order. The enhancement of the Fermi-surface effect in the Pt-Mn alloys occurs as a result of an atomic order, which has never been observed in other alloys. We attribute this new phenomenon to the characteristic feature of the $ABC_6$ type structure, since it dose not occur in the ordered Pt-Mn alloys with the $Cu_3Au$ type structure. The present model is too simplified to explain the fourfold splitting, which may arise from the complicated structure of the nesting Fermi surface. A calculation of the energy band structure with a proper method is necessary for a explanation of the fourfold splitting.

The result of the annealed #1 sample of 14.4 at.%Mn indicates that the short-ranged SDW which originated by the enhanced Fermi-surface nesting effect is also formed in the Pt-Mn alloys with the $ABC_6$ type ASRO whose atomic correlation length is rather long. On the other hand, the SDW remains to be short-ranged, even if the $ABC_6$ type long-range order develops in the Pt-Mn alloys. The correlation length of the SDW is only about one period of the modulation in the [110] directions ($\sim 17a_0$) for the two annealed samples of 12.5 at.%Mn. In the annealed #2 sample of 12.5 at.%Mn, another set of diffuse peaks appears at $1/2,\pm 1/4,0$, $1/2,0,\pm 1/4$ and their equivalent points. In the annealed #2 sample of 14.4 at.%Mn, the fourfold splitting of the diffuse scattering disappears completely, and these new peaks grow up to be sharp superlattice reflections. These results indicate that the SDW is disturbed by the commensurate magnetic structure, which is more stable in the $ABC_6$ type long-range order with a higher Mn concentration.

For the superlattice peaks in the annealed #2 sample of 14.4 at.%Mn, it should be noted that they are also centered at $1/2,0,0$. The magnetic structure is thus regarded to have antiparallel alignment for successive (100) planes of Mn atoms, with a commensurate modulation of $4a_0$ (or twice of that of $ABC_6$ type unit lattice ) parallel to the cubic axis in the plane. Since the intensities of the peaks at $1/2,\pm 1/4,0$ and $1/2,0,\pm 1/4$ are different, these peaks come from different magnetic domains, i.e., an antiparallel alignment along [100] with the modulation along [010] and one with the modulation along [001]. Therefore, the magnetic structure consists of 12 domains with an anisotropic distribution. The origin of the magnetic structure is not the distant interaction through the SDW in the conduction-electron gas, but an antiferromagnetic interaction between the near-neighbor localized spins. In the $ABC_6$ type structure with a Mn concentration lower than 12.5 at.%, Mn occupies alternate corner sites (A sublattice), where the distance between the nearest neighbors of $\sqrt{2}a_0$ seems to be too large to cause a strong interaction between them. However, if the excess Mn atoms occupy the other corner sites (B sublattice) in the 14.4 at.%Mn, the Mn-Mn interaction becomes much stronger through the magnetic moment induced by the small occupation probability of Mn on the B sublattice. This is a possible interpretation based on our previous results for the $ABC_6$ type structure, in which the A and B sublattices are not crystallographically equivalent in the ordered structure.[1] This is considered to be the reason why the magnetic structure is long ranged only in the annealed #2 sample of 14.4 at.%Mn. Since diffuse scattering is still observed around the superlattice points at $2T_N$, the short-ranged magnetic structure is formed from far above $T_N$. The remanence from RT observed for the $\chi(T)$ in the sample may be related to this local magnetic structure.

The superlattice peaks disappear in the 15.9 at.%Mn samples, indicating a rapid change in the magnetic structure with the Mn concentration. This corresponds to the fact that the $ABC_6$ type atomic order exists in a very narrow concentration region, and the $Cu_3Au$ type order rapidly becomes dominant for the more concentrated alloys. The $Cu_3Au$ type ordered $Pt_3Mn$ alloy is a ferromagnet with its Curie temperature being at 390 K.[27] The related ferromagnetic correlation develops with the development of the $Cu_3Au$ type order. In the present samples, the correlation cannot be long ranged, even if the $Cu_3Au$ type ALRO develops. This is considered to be due to the low degree of the atomic order in the samples.

We have discussed three different interactions for the magnetic scattering: SDW, antiferromagnetic (AF), and ferromagnetic (F) interactions. In Table IV, the dominant interaction is indicated for each scattering. In the present argument, it is assumed that the magnetic moments are on the localized 3*d* electrons of Mn, and two extreme cases are considered: one where an interaction through the conduction electrons is dominant, and the other where a direct *d–d* interaction is dominant. Actually, the interaction between the 3*d* and conduction electrons always exists, and should be taken into account for the latter case. For a quantitative discussion, theoretical efforts are expected for the Pt-Mn alloy system to treat both interactions appropriately.

### B. SDW and spin-glass-like behavior

The magnetic susceptibility shows the same characteristics of the spin-glass-like behavior in all of the samples, implying that the fluctuating SDW clusters proposed by Tsunoda *et al.* exist throughout the observed magnetic structures.[9,16] With the development of the $ABC_6$ type order, we have noticed that the freezing temperature tends to be lower and the SDW diffuse intensities appear at lower temperature. These results indicate that the fluctuation of SDW clusters is suppressed with the development of the $ABC_6$ type order. This is attributed to competition between the SDW and antiferromagnetic interactions. It should be pointed out that both SDW short-range and antiferromagnetic long-range orders have a component of the propagation vector of $1/2,0,0$. A slight difference in the atomic order would greatly change the magnetic interaction, and cause different modulations in the plane vertical to the propagation vector. Therefore, the magnetic structures are easy to be disturbed by atomic arrangements and the SDW fluctuations may survive dynamically through these structures. To confirm this dynamical fluctuation, studies with inelastic neutron scattering are necessary and are now in progress.

For the higher Mn concentration, the $Cu_3Au$ order develops and the ferromagnetic interaction on the structure becomes dominant. In contrast to the $ABC_6$ type structure, the development of the $Cu_3Au$ type structure does not seem to suppress the spin-glass-like behavior. $T_g$ rises continuously with the development of the structure. In fact, we examined $\chi(T)$ in 17 and 20 at.%Mn, and found that the spin-glass-like behavior still exists in these samples with $T_g$ being $\sim$48 and $\sim$80 K, respectively, though cusps are quite smeared. It seems that the magnetic structure changes from the SDW short-range order to the ferromagnet one continuously. In other words, if it were not for the $ABC_6$ type ordered phase in Pt-Mn alloys, the position of the SDW diffuse peak would simply shift from $1/2,0,0$ to $1,0,0$ with increasing the Mn concentration, and it would become ferromagnetic scattering at around 25 at.%Mn, as observed in other Pt- and Pd-M alloys. Considering that the $ABC_6$ type ASRO is observed in the disordered alloys with a wide range of low Mn concentration, the persistence of the SDW diffuse peaks at $1/2,0,0$ in these samples can also be related to the existence of the $ABC_6$ type phase in the Pt-Mn alloys.

## V. CONCLUSION

The magnetism in Pt-rich Pt-Mn alloys was studied by neutron-diffraction and magnetic-susceptibility measurements. The magnetic susceptibility showed a spin-glass-like behavior for all of the samples. In neutron scattering, two kinds of magnetic structure were found in samples with the $ABC_6$ type structure, both of which are characterized by a propagation vector of $1/2,0,0$. However, in the plane vertical to the vector, one has an incommensurate modulation parallel to the diagonal direction of the cubic axis, and the other has a commensurate modulation parallel to the cubic axis. The former is due to the interaction between the distant localized spins through the SDW in the conduction-electron gas, and is enhanced in the narrower Brillouin zone of this

structure, while the latter is due to the interaction between the near-neighbor localized Mn spins, and is more dominant in the $ABC_6$ type structure. With the development of the $Cu_3Au$ type order and higher Mn concentration, the dominant interaction changes to a ferromagnetic one arising from the ferromagnetic $Pt_3Mn$. The variation in the magnetic structure is closely related to the characteristic atomic order of the $ABC_6$ type in the alloys, showing a strong coupling between the magnetic and atomic structures.

## ACKNOWLEDGMENTS

We would like to express our thanks to T. Sugawara for Advanced Materials, Institute for Materials Research, Tohoku University for help in growing single crystals and to K. Nishida of the Chemical Analysis Center, University of Tsukuba for his assistance in EPMA. We wish to acknowledge Dr. S. Suzuki for calculating the energy band structure of the Pt-Mn alloy. We are also grateful to Professor K. Kadowaki and Professor K. Motoya for their valuable discussions and Professor M. Arai for his advice on neutron-scattering measurements at KENS. The present work was supported in part by 21st Century COE (Center of Excellence) Program "Promotion of Creative Interdisciplinary Materials Science for Novel Functions" and also by a Grant-in-Aid for Young Scientists (B) (KAKENHI, No. 15760487) under MEXT (the Ministry of Education, Culture, Sports, Science and Technology), Japan.

*Present address: Department of Physics, Faculty of Mathematics and Natural Science, University of Sumatera Utara, Medan, Indonesia.

[1] M. Takahashi, T. Sembiring, M. Yashima, T. Shishido, and K. Ohshima, J. Phys. Soc. Jpn. **71**, 681 (2002).
[2] T. Sembiring, M. Takahashi, K. Ota, T. Shishido, and K. Ohshima, J. Phys. Soc. Jpn. **71**, 2459 (2002).
[3] T. Sembiring, D. K. Saha, M. Takahashi, T. Shishido, and K. Ohshima, J. Phys. Soc. Jpn. **72**, 107 (2003).
[4] Y. Tang, Acta Crystallogr. **4**, 377 (1951).
[5] A. G. Khachaturyan, Prog. Mater. Sci. **22**, 75 (1978).
[6] E. F. Wassermann, Physica B & C **109–110**, 1936 (1982).
[7] J. W. Cable, S. A. Werner, G. P. Felcher, and N. Wakabayashi, Phys. Rev. B **29**, 1268 (1984).
[8] S. A. Werner, Comments Condens. Matter Phys. **15**, 55 (1990).
[9] Y. Tsunoda and J. W. Cable, Phys. Rev. B **46**, 930 (1992).
[10] S. A. Werner, J. J. Rhyne, and J. A. Gotaas, Solid State Commun. **56**, 457 (1985).
[11] J. A. Gotaas, J. J. Rhyne, and S. A. Werner, J. Appl. Phys. **57**, 3404 (1985).
[12] Y. Tsunoda, N. Kunitomi, and J. W. Cable, J. Appl. Phys. **57**, 3753 (1985).
[13] J. W. Cable and Y. Tsunoda, J. Appl. Phys. **73**, 5454 (1993).
[14] Y. Tsunoda, J. Magn. Magn. Mater. **177-181**, 1337 (1998).
[15] Y. Tsunoda and R. Abe, Phys. Rev. B **55**, 11507 (1997).
[16] Y. Tsunoda, N. Hiruma, J. L. Robertson, and J. W. Cable, Phys. Rev. B **56**, 11051 (1997).
[17] M. Hirano and Y. Tsunoda, Phys. Rev. B **59**, 13835 (1999).
[18] Y. Tsunoda, M. Hirano, M. L. Crow, and J. L. Robertson, Phys. Rev. B **62**, 5570 (2000).
[19] Y. Tsunoda, A. Harigae, J. L. Robertson, and M. L. Crow, Phys. Rev. B **62**, 9511 (2000).
[20] M. Takahashi, S. Yoshimi, K. Ohshima, and Y. Watanabe, Phys. Rev. B **61**, 3528 (2000).
[21] M. Takahashi, M Hashimoto, K. Ohshima, Y. Noda, N. Takesue, and T. Shishido, J. Phys. Soc. Jpn. **70**, Suppl. A, 136 (2001).
[22] O. K. Andersen and A. R. Mackintosh, Solid State Commun. **6**, 285 (1968).
[23] M. Takahashi (unpublished).
[24] Y. Noda, H. Kimura, R. Kiyanagi, A. Kojima, Y. Morii, N. Minakawa, and N. Takesue, J. Phys. Soc. Jpn. **70**, Suppl. A, 456 (2001).
[25] We have examined the shape of Fermi surface for the $ABC_6$ type ordered Pt-12.5 at.%Mn with a simple model of ferromagnetic state by a fully relativistic full-potential LCAO method [S. Suzuki and K. Nakao, J. Phys. Soc. Jpn. **68**, 1982 (1999)]. The calculation shows a set of nearly parallel planes normal to the cubic axis in the hole Fermi surface, similar to the one in pure Pt.
[26] S. C. Moss, Phys. Rev. Lett. **22**, 1108 (1969).
[27] E. Krén, G. Kádár, L. Pál, J. Sólyom, P. Szabó, and T. Tarnóczi, Phys. Rev. **171**, 574 (1968).